

# Crystal structure prediction of organic pigments: quinacridone as an example

N. Panina,<sup>a</sup> F. J. J. Leusen,<sup>b</sup> F. F. B. J. Janssen,<sup>a</sup> P. Verwer,<sup>c</sup> H. Meekes,<sup>a\*</sup> E. Vlieg<sup>a</sup> and G. Deroover<sup>d</sup>

<sup>a</sup>IMM Dept. for Solid State Chemistry, Radboud University Nijmegen, Toernooiveld 1, 6525 ED Nijmegen, The Netherlands, <sup>b</sup>IPI, University of Bradford, Bradford, West Yorkshire, BD7 1DP, UK, <sup>c</sup>Akzo Nobel Chemicals BV, Dept. CPT, PO Box 9300, 6800 SB Arnhem, The Netherlands, and <sup>d</sup>Agfa-Gevaert NV, Septestraat 27, B-2640 Mortsel, Belgium. Correspondence e-mail: hugo.meekes@science.ru.nl

The structures of the  $\alpha$ ,  $\beta$  and  $\gamma$  polymorphs of quinacridone (Pigment Violet 19) were predicted using *Polymorph Predictor* software in combination with X-ray powder diffraction patterns of limited quality. After generation and energy minimization of the possible structures, their powder patterns were compared with the experimental ones. On this basis, candidate structures for the polymorphs were chosen from the list of all structures. Rietveld refinement was used to validate the choice of structures. The predicted structure of the  $\gamma$  polymorph is in accordance with the experimental structure published previously. Three possible structures for the  $\beta$  polymorph are proposed on the basis of X-ray powder patterns comparison. It is shown that the  $\alpha$  structure in the Cambridge Structural Database is likely to be in error, and a new  $\alpha$  structure is proposed. The present work demonstrates a method to obtain crystal structures of industrially important pigments when only a low-quality X-ray powder diffraction pattern is available.

© 2007 International Union of Crystallography  
 Printed in Singapore – all rights reserved

## 1. Introduction

A pigment is a coloured organic or inorganic solid that is usually insoluble in its application media. Pigments are used when extreme resistance to light, weather or temperature is needed, *e.g.* in automotive paints and other outdoor applications. Due to its insolubility, a pigment will usually retain its crystal structure throughout the preparation and application process. Various physico-chemical properties of pigments, including colour, thermal stability, particle shape, light fastness and fluorescence, are dependent on the crystal packing of the pigment molecules.

Despite the commercial significance of non-azo organic pigments, only few full crystal structures of these materials have been reported, because single crystals are hard to obtain. Pigments are practically insoluble, thus solution growth methods are inappropriate. Pigments are produced by precipitation reactions leading to very fine powders. The crystallites are often so small that they lead to considerable line broadening in X-ray powder diffraction. Single-crystal growth by sublimation methods, on the other hand, rarely produces crystals of suitable quality for conventional X-ray single-crystal structure determination. As a result, the important crystallographic features, controlling the crystal chemistry of such materials, have remained unknown for many pigments.

The purpose of this research is to study the feasibility of obtaining the crystal structures of the polymorphs of pigments

with the aid of crystal structure prediction (CSP) tools in combination with limited experimental data. A similar approach was reported by Erk (2001) and Schmidt *et al.* (2005). One can obtain a good impression of the state-of-the-art in crystal structure prediction by looking at the results of CSP tests organized in recent years by the Cambridge Crystallographic Data Centre (see Day *et al.*, 2005, and references therein). Three CSP 'blind tests' in 1999, 2001 and 2004 indicated that certain progress has been made in the *ab initio* prediction of structures of 'small' (not more than 25 atoms) rigid molecules containing only C, H, N and O atoms.

As an example of an insoluble pigment with poor crystal quality, unsubstituted linear *trans*-quinacridone, often called quinacridone (QA), a parent compound of various related pigments (Fig. 1), was chosen. A review on various quinacridone-related compounds has been given by Lincke (2000). In

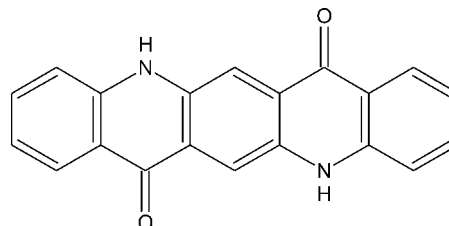


**Figure 1**  
 Linear *trans*-quinacridone.

patent reports, at least six polymorphic forms of quinacridone have been reported on the basis of X-ray powder data (Reidinger & Struve, 1955; Struve, 1955; Manger & Struve, 1957; Filho & Oliveira, 1992). Only three of them,  $\alpha$ ,  $\beta$  and  $\gamma$ , are widely accepted. The crystal structure of the  $\gamma$  polymorph (Mizuguchi *et al.*, 2002) is available from the Cambridge Structural Database (CSD), while for the  $\beta$  polymorph only the cell parameters, space group and a powder pattern have been published (Paulus *et al.*, 1989; Struve, 1955). The structure of the  $\alpha$  polymorph, derived through calculations and reported in the CSD (Lincke & Finzel, 1996), is likely to be incorrect, as discussed later. Thus, this structural information was not used further in our work. Crystal structure prediction of quinacridone polymorphs has been mentioned previously (Leusen, 1996) by Accelrys (formerly Molecular Simulations Ltd) as an example of the use of the *Cerius<sup>2</sup> Polymorph Predictor*, but the details of the prediction and the resulting structures remained unpublished.

## 2. Materials and methods

### 2.1. Experimental methods

The pure  $\beta$  and  $\gamma$  polymorphs of QA were provided by Agfa-Gevaert NV and used as received. The powder of  $\alpha$ -QA was obtained by slow water dilution of a concentrated H<sub>2</sub>SO<sub>4</sub> solution of QA. For that, a solution of  $\gamma$ -QA in concentrated sulfuric acid was placed in one test tube and water in a second one. The tubes were connected with each other and the water tube was heated to increase the water vapour pressure in the system. After the precipitation of a dark violet powder in the sulfuric acid solution, the mixture was filtered and the powder of  $\alpha$ -QA was collected and dried. X-ray powder diffraction (XRPD) patterns of the samples were obtained using a Philips PW 1710 diffractometer by scanning the samples over  $2\theta$  angles ranging from 2 to 35°, using Cu  $K\alpha$  radiation with wavelength 1.5418 Å.

### 2.2. Computational methods

Crystal structure prediction was conducted using the Accelrys *Polymorph Predictor* (PP) module in the *Cerius<sup>2</sup>* package (Accelrys, 2002). In short, this program generates randomly a number of crystal packings in a chosen space group. The energy of these structures is minimized using molecular mechanics force fields. These structures are subsequently ranked, *e.g.* according to the lattice energy. The structures that are highest in rank are expected to have the highest probability of being found experimentally. For more details on the theory and background of the prediction procedures implemented in the PP, refer to the work of Gdanitz *et al.* (1993) and Karfunkel *et al.* (1993, 1994).

The molecule of quinacridone was first drawn in the three-dimensional sketcher and then energetically minimized in the Dreiding 2.21 force field. Electrostatic potential derived (ESPD) point charges were assigned to the atoms in the molecule. These charges were obtained by *ab initio* Hartree–Fock calculations at the given molecular geometry using the

quantum mechanics program *GAUSSIAN94* (Frisch *et al.*, 1998) with the 6-31G\* basis set. Before starting the prediction procedure, the geometry of the molecule was optimized again in the force field, but this did not contribute any significant changes to the geometry.

The Dreiding 2.21 force field was also used to minimize the energy of the crystal structures in the final step of the PP procedure. The calculation of the van der Waals and Coulomb interactions was performed using the Ewald summation method; the dielectric constant  $\epsilon_r$  was kept constant (unlike the default *Cerius<sup>2</sup>* setting of distance proportionality).

Rietveld refinement was performed using the *DBWS-9006* program (Wiles & Young, 1981), implemented in *Cerius<sup>2</sup>*. The refinement was performed in the range of  $2\theta$  from 2 to 35°. Only the scale factor, background, cell parameters and the peak profile parameters were varied; the fractional atomic coordinates were kept fixed at this stage. The atomic coordinates were optimized by lattice energy minimization with fixed unit-cell parameters between the Rietveld steps.

### 2.3. Crystal structure prediction procedure

*Ab initio* structure prediction is usually conducted in the space groups most frequently found among organic solids. 18 space groups together account for more than 93% of the molecular crystals reported (Baur & Kassner, 1992). However, since the space groups of quinacridone polymorphs are already known from the literature [ $P\bar{1}$  for  $\alpha$ -QA (although questionable) and  $P2_1/c$  for  $\beta$  and  $\gamma$ -QA], we used this knowledge to limit the choice of the space groups. The flat and rigid molecule of quinacridone has an inversion centre. As intramolecular symmetry is not recognized during the PP prediction process, the prediction should be done in a space group that is a subgroup of the desired space group; the inversion centre is expected to be part of the symmetry elements of the space group. For the present case, the subgroup should contain all symmetry elements of the desired group, excluding the inversion centre. Therefore, we conducted the search in the space groups  $P1$ ,  $P2_1$  and  $Pc$  only. It is not necessary to search in all three subgroups: with a sufficient number of trials all  $P2_1/c$  structures will be found among the structures of each of these subgroups. For practical reasons (to reduce the calculation time), the search was conducted in all three subgroups and the results were subsequently merged.

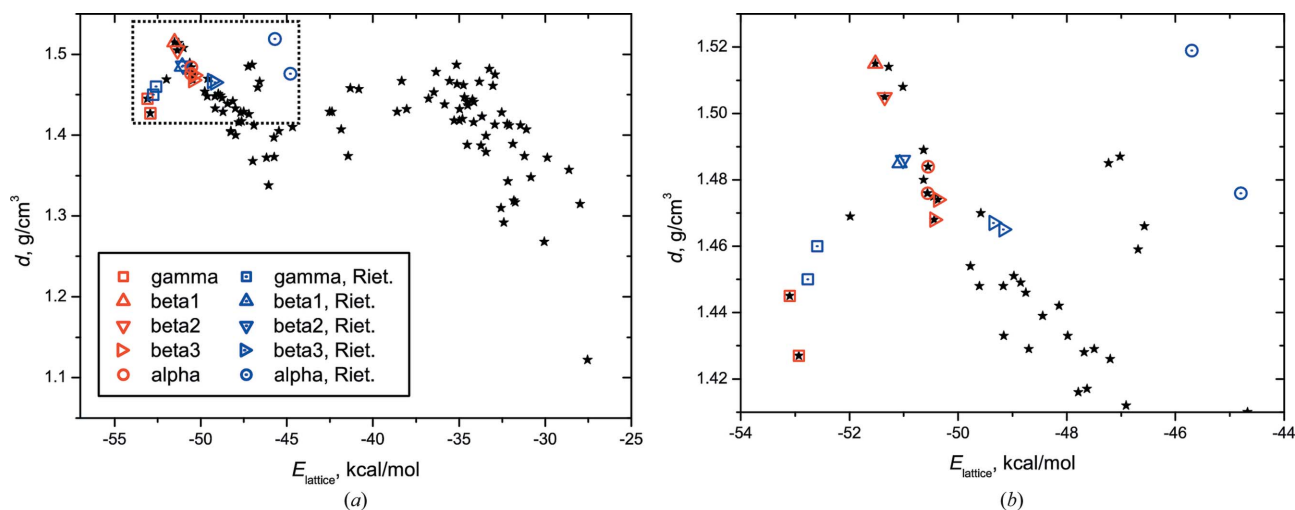
A single quinacridone molecule was placed in the asymmetric unit. A total of 2000 trial structures were generated in each space group. Then, the clustering algorithm was applied to remove duplicate structures which resulted in total of 497 structures. Minimization of the total potential energy was then performed on the remaining structures, now also relaxing the rigid-body constraints. After clustering of the minimized structures, 61 structures remained. After the prediction process, an additional step was performed to find the actual symmetry (with the *Find Symmetry* tool) followed by a further energy minimization of the crystal structures in the space group found if it differed from the initial space group. The

**Table 1**

Fifteen low-energy predicted structures ranked with respect to the lattice energy.

Besides crystallographic details, the density and the lattice energies are given. The column 'Crystal form' gives the assignment of the structure to known polymorphs on the basis of available XRPD patterns; structures that are not assigned have powder patterns which show no resemblance with the experimental ones. The structures in bold were subsequently subjected to Rietveld refinement.

No.	Space group	Cell axes			Cell angles			$d$ (g cm <sup>-3</sup> )	$E_{\text{lattice}}$ (kcal mol <sup>-1</sup> )	Crystal form
		$a$ (Å)	$b$ (Å)	$c$ (Å)	$\alpha$ (°)	$\beta$ (°)	$\gamma$ (°)			
<b>1</b>	<b><math>P2_1/c</math></b>	<b>14.130</b>	<b>4.008</b>	<b>13.424</b>	<b>90</b>	<b>70.77</b>	<b>90</b>	<b>1.445</b>	<b>-53.098</b>	$\gamma$
<b>2</b>	<b><math>P2_1/c</math></b>	<b>14.255</b>	<b>3.824</b>	<b>13.671</b>	<b>90</b>	<b>77.31</b>	<b>90</b>	<b>1.427</b>	<b>-52.930</b>	$\gamma$
3	$P2_1/c$	11.348	6.280	13.031	90	130.48	90	1.469	-51.986	—
<b>4</b>	<b><math>P2_1/c</math></b>	<b>5.734</b>	<b>3.966</b>	<b>31.096</b>	<b>90</b>	<b>104.51</b>	<b>90</b>	<b>1.515</b>	<b>-51.522</b>	$\beta_1$
<b>5</b>	<b><math>P2_1/c</math></b>	<b>3.988</b>	<b>5.720</b>	<b>30.288</b>	<b>90</b>	<b>94.04</b>	<b>90</b>	<b>1.505</b>	<b>-51.352</b>	$\beta_2$
6	$P2_1$	28.184	4.933	4.977	90	81.94	90	1.514	-51.278	—
7	$P2_1/c$	5.019	4.891	28.088	90	94.05	90	1.508	-51.015	—
8	$P\bar{1}$	5.924	16.784	3.809	109.91	91.51	100.58	1.489	-50.634	$\alpha$
9	$P\bar{1}$	15.767	3.874	5.813	89.67	95.71	97.23	1.480	-50.633	$\alpha$
<b>10</b>	<b><math>P\bar{1}</math></b>	<b>6.922</b>	<b>3.873</b>	<b>14.770</b>	<b>85.27</b>	<b>85.57</b>	<b>63.07</b>	<b>1.476</b>	<b>-50.563</b>	$\alpha$
<b>11</b>	<b><math>P\bar{1}</math></b>	<b>6.271</b>	<b>3.935</b>	<b>15.019</b>	<b>80.49</b>	<b>73.91</b>	<b>81.94</b>	<b>1.484</b>	<b>-50.555</b>	$\alpha$
12	$P2_1$	3.887	29.214	6.920	90	116.52	90	1.475	-50.451	$\alpha$
<b>13</b>	<b><math>P2_1/c</math></b>	<b>5.745</b>	<b>31.288</b>	<b>3.931</b>	<b>90</b>	<b>90.29</b>	<b>90</b>	<b>1.468</b>	<b>-50.440</b>	$\beta_3$
<b>14</b>	<b><math>P2_1</math></b>	<b>3.837</b>	<b>31.228</b>	<b>5.874</b>	<b>90</b>	<b>89.18</b>	<b>90</b>	<b>1.474</b>	<b>-50.373</b>	$\beta_3$
15	$P2_1/c$	15.887	7.013	31.143	90	11.87	90	1.454	-49.773	—

**Figure 2**

(a) Results of the polymorph prediction as an energy-density distribution plot. Each star represents one predicted structure. The structures assigned to known polymorphs on the basis of powder patterns are marked with red symbols. Rietveld-refined structures of red-marked structures are represented by corresponding blue symbols. (b) Detailed view of the top-left area of (a).

latter step is necessary to reach the optimal structure in the space group found, as the atomic coordinates obtained by imposing the new symmetry may not correspond exactly to an energy minimum, in particular in the case of intramolecular symmetry, where small deviations in bond lengths lead to a substantial increase in energy. As the prediction procedure contains a Monte Carlo stage, it can give different results for different runs. Three runs were enough to obtain reproducible results.

In order to evaluate the polymorph prediction results, X-ray powder diffraction patterns of the predicted structures were calculated and compared with the experimental ones. Due to the limited amount of predicted structures, it was possible to conduct the comparison manually for every structure. The quality of the experimental data was not good enough for indexing the patterns and deducing the structure, but sufficient to evaluate the PP results. The structures with powder patterns

closest to the experimental ones were subjected to the Rietveld refinement.

### 3. Results

The prediction, as a result of three consecutive runs, ended with 103 structures ranging in lattice energy from -53 to -28 kcal mol<sup>-1</sup> (1 cal = 4.184 J). Fig. 2 shows the predicted structures in terms of their lattice energy and density. We used density as a parameter to present the results in a clearer way and to distinguish structures with the same energy. A higher density might suggest a more stable structure, but this indicator is not as strong as low lattice energies.

Table 1 gives the information of the first 15 low-energy structures sorted with respect to the lattice energy. The last column shows the attribution of the structures to known polymorphs on the basis of the XRPD pattern. Structures in

**Table 2**

Crystallographic data of predicted quinacridone polymorphs after Rietveld refinement and known experimental data for  $\gamma$  (Mizuguchi *et al.*, 2002) and  $\beta$  (Paulus *et al.*, 1989) polymorphs.

The numbers labelling the predicted structures refer to the entries of Table 1.

	$\gamma$ (No. 2)	$\gamma$ -exp	$\beta_1$ (No. 4)	$\beta_2$ (No. 5)	$\beta_3$ (No. 13)	$\beta$ -exp	$\alpha$ (No. 10)
Space group	$P2_1/c$	$P2_1/c$	$P2_1/c$	$P2_1/c$	$P2_1/c$	$P2_1/c$	$P\bar{1}$
$a$ (Å)	13.998	13.700	5.621	4.057	5.557	5.692	6.748
$b$ (Å)	3.890	3.840	4.059	5.622	30.674	3.975	3.776
$c$ (Å)	13.383	13.350	31.177	30.938	4.149	30.02	14.400
$\alpha$ (°)	90	90	90	90	90	90	85.34
$\beta$ (°)	79.04	100.09	100.94	98.17	89.00	96.76	81.76
$\gamma$ (°)	90	90	90	90	90	90	70.20
$Z$	2	2	2	2	2	2	1
$V$ (Å <sup>3</sup> )	716	691	698	696	707	675	341
$d$ (g cm <sup>-1</sup> )	1.450	1.485	1.485	1.486	1.467	1.447	1.519

bold are considered to be close enough to the experimental structures to serve as input for the Rietveld refinement. The resulting structures after the Rietveld refinement are shown in Fig. 2. Table 2 gives the crystallographic data of the refined structures and published experimental data on  $\beta$ - and  $\gamma$ -QA for comparison.

**4. Discussion**

We only consider the three widely accepted polymorphs ( $\alpha$ ,  $\beta$ ,  $\gamma$ ), which have distinct powder patterns. Additional crystal phases mentioned in patents were reported on the basis of powder patterns of poor quality, giving rise to quite some

uncertainty concerning their existence. Moreover, one of these phases, designated as  $\gamma'$  (Deuschel *et al.*, 1963), was proven to be  $\gamma$ -QA. Variations in the crystallite size and shape caused, in this case, the differences in the powder patterns (Potts *et al.*, 1994).

**4.1.  $\gamma$ -Quinacridone**

The structure of the  $\gamma$  polymorph, determined by single-crystal X-ray measurements, is known from the CSD (reference code QNACRD04). The prediction of this structure served as a

test to evaluate the quality of the force field and polymorph prediction in general.

Structures 1 and 2 in Table 1 have powder patterns similar to the experimental one (Fig. 4). Both structures agree with the experimental crystal structure from the CSD. The difference between the structures is so small that they can be considered to represent the same structure. Thus, the structure of  $\gamma$ -QA is predicted correctly and as the global minimum. The molecular packing of  $\gamma$ -QA is shown in Fig. 3. Each quinacridone molecule forms hydrogen bonds with four neighbours and they are packed in a criss-cross manner in ribbons along [001].

Rietveld refinement performed on both structures resulted in  $R$  factors of 18.5 and 14.1% (structures 1 and 2, respec-

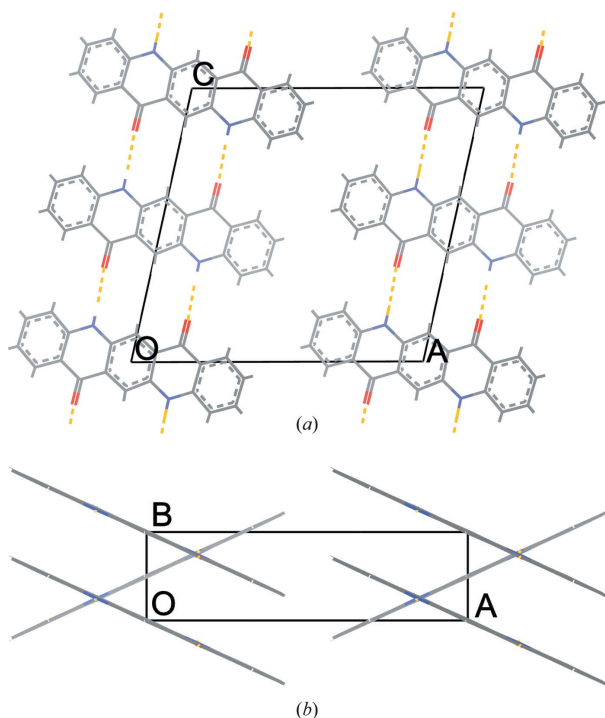


**Figure 3**  
Two projections of the predicted crystal structure of  $\gamma$ -QA. Dashed yellow lines represent hydrogen bonds. In the view along the  $c$  axis, hydrogen bonds are perpendicular to the plane of the picture, connecting four neighbouring molecules to each quinacridone molecule at the crossing points.

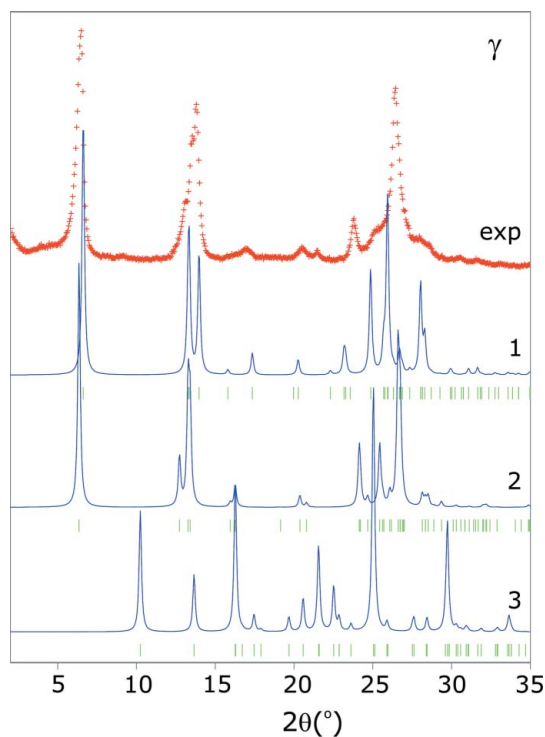


**Figure 4**  
Powder patterns of structures 1, 2 and 3 of Table 1 compared with the experimental powder pattern of  $\gamma$ -QA; structure 3 is added to show the large dissimilarity.

tively) and nearly the same final structure. In Table 2, we cite data for the second structure, as it showed a better Rietveld fit. As a test, the experimental structure QNACRD04 was refined against our experimental powder data in the same way as it was for the predicted structure. The  $R$  factor of the fit was 10.8%, a value which is an indication for the order of the accuracy of fits for the other predicted structures, given the limited quality of the experimental powder diffraction pattern.

#### 4.2. $\beta$ -Quinacridone

In spite of the commercial significance of  $\beta$ -QA and many attempts to grow single crystals, its structure is still unknown in the open literature. At present, only the cell parameters, the space group and a sketchy powder pattern are available (Paulus *et al.*, 1989; Struve, 1955). According to these data,  $\beta$ -QA has a monoclinic structure, space group  $P2_1/c$  and cell parameters as listed in Table 2.

The polymorph prediction resulted in several structures for  $\beta$ -QA; all fit the experimental powder pattern well (Fig. 5). However, none of the predicted structures reproduces the small peak at  $14^\circ$  in the experimental pattern, which can be attributed to an impurity.

Structure 4, designated here as  $\beta_1$ , is monoclinic, space group  $P2_1/c$ , and has a long  $c$  axis ( $\sim 31$  Å). Each molecule forms hydrogen bonds with two neighbours, forming ribbons

that are arranged in two directions, along  $[110]$  and  $[\bar{1}\bar{1}0]$  (Fig. 6). The cell parameters of this structure fit well to the data reported in the literature (Table 2).

Structure 5, which is labelled as  $\beta_2$ , has the same molecular packing and a similar unit cell as structure 4, though their cell lengths do not correspond. The packing is shown in Fig. 7. The distances between the planes of the molecules in the stacks in these two structures,  $\beta_1$  and  $\beta_2$ , are 2.86 Å and 2.89 Å, and the angles between molecules in different stacks are  $60.2^\circ$  and  $60.3^\circ$ , respectively. This may give the impression that the structures are defined in different settings of the space group  $P2_1/c$  and that they can be adjusted to have the same cell parameters. However, the unique axis 3.988 Å in the  $\beta_1$  structure clearly differs from its value of 5.720 Å in the  $\beta_2$  structure. This shows that these two structures are indeed different.  $\beta_1$ -QA has somewhat lower lattice energy and higher density as compared with  $\beta_2$ -QA.

Structures 13 and 14 are similar but defined in different space groups. Structure 13 is monoclinic, space group  $P2_1/c$ . Structure 14 has nearly the same arrangement of molecules and cell parameters as structure 13, but in space group  $P2_1$ , which is quite uncommon for a molecule with inversion symmetry. Both structures are designated here as  $\beta_3$ . The unit-cell axes lengths of  $\beta_3$  are comparable with the two previously mentioned  $\beta$  structures, but the unique axes differ (Table 1). The crystal structures of  $\beta_3$  resemble that of  $\beta_1$  and  $\beta_2$  with the difference that the stacks of hydrogen-bonded molecules are arranged in a nearly parallel way, along  $[\bar{1}01]$  (Fig. 8). The hydrogen-bond patterns are similar for all the  $\beta$  structures; each molecule has four hydrogen bonds to two neighbouring molecules and the resulting ribbons are packed in stacks.

Rietveld refinement of the  $\beta_1$  and  $\beta_2$  structures against the experimental powder pattern resulted in both cases in a reasonable fit with  $R$  values of 13.0 and 12.6%, respectively. The difference can be noted at  $15^\circ$  in Fig. 5, where  $\beta_1$  has two peaks and  $\beta_2$  only one. The corresponding peak in the experimental pattern is broad and makes it impossible to distinguish between these two structures. It is notable that both refined structures are very close in the energy density plot (Fig. 2*b*). Both structures of  $\beta_3$  undergo cell compression during the Rietveld refinement due to the shortening of the long axis. The energy minimization performed between the Rietveld steps forces molecules to leave the nearly parallel arrangement of stacks (see Fig. 9). The density is nevertheless hardly affected (Fig. 2*b*). The refinement converges at  $R$  values of 19.7% and 20.6% for the structures 13 and 14, respectively, and leads to nearly the same structure in both cases. Therefore, only the crystallographic data for the refined structure 13 are listed in Table 2.

As a result of the Rietveld refinement,  $\beta_1$  and  $\beta_2$  show better similarity with the experimental powder pattern, and the published data favour the  $\beta_1$  structure. However, considering that  $R_{\text{exp}}$  of the  $\beta$  structure reported by Paulus *et al.* (1989) is not known and that the energies of all three  $\beta$  structures mentioned here are within the error of the prediction (a few kcal mol $^{-1}$ ), each of them remains a candidate for the experimental structure.

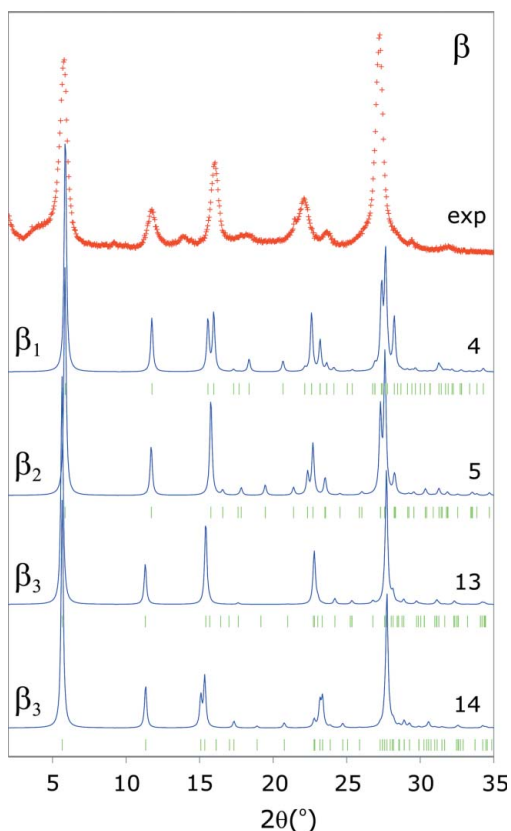


**Figure 5**  
Powder patterns of structures 4, 5, 13 and 14 of Table 1 compared with the experimental powder pattern of  $\beta$ -QA.

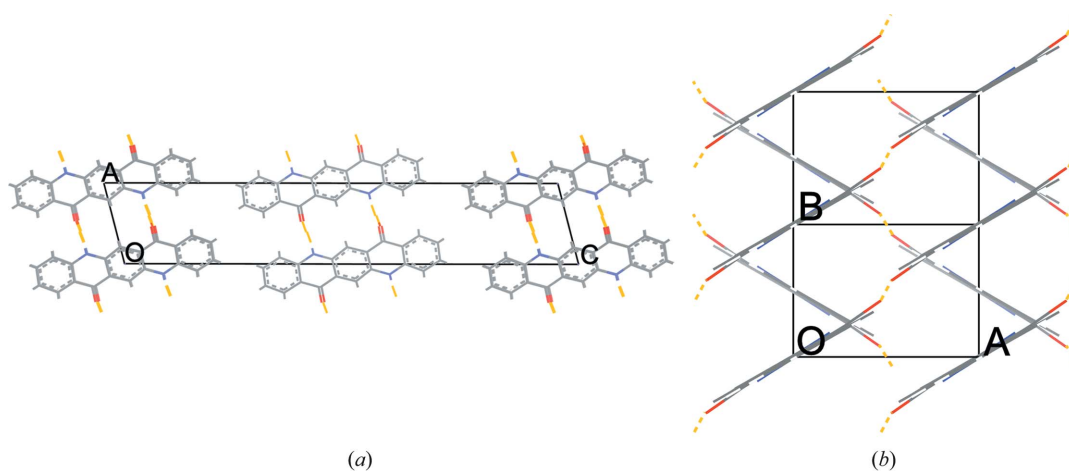


**Figure 6**  
Two projections of the predicted crystal structure of  $\beta_1$ -QA: views along the short and long axes. Dashed yellow lines represent hydrogen bonds. The projection along the  $c$  axis shows that each molecule is connected to two neighbouring molecules *via* hydrogen bonds.

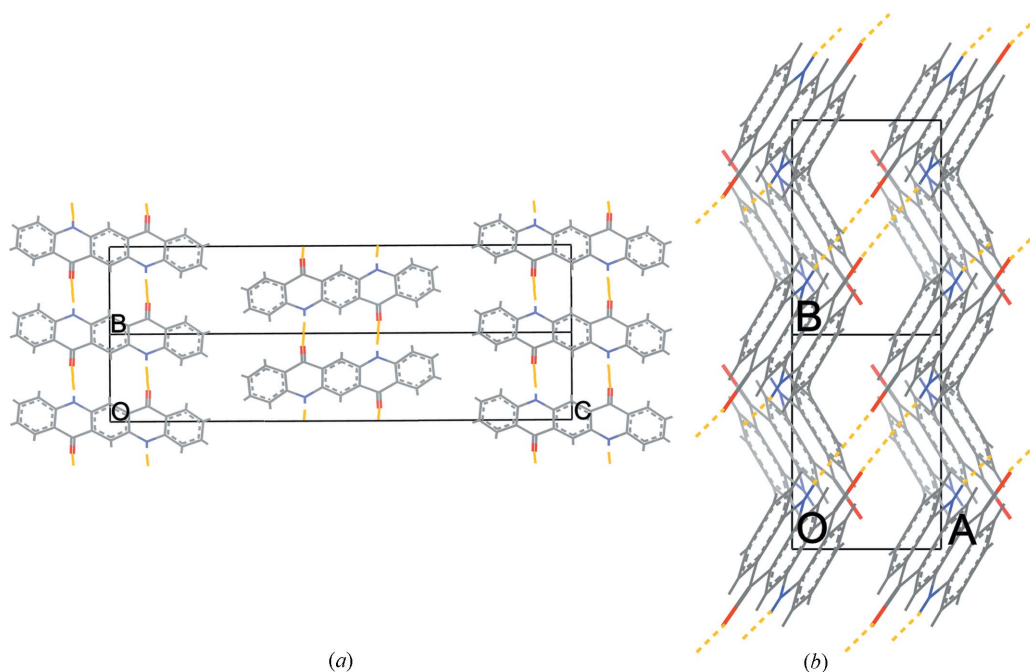


**Figure 7**  
Two projections of the predicted crystal structure of  $\beta_2$ -QA: views along the short and long axes. Dashed yellow lines represent hydrogen bonds.

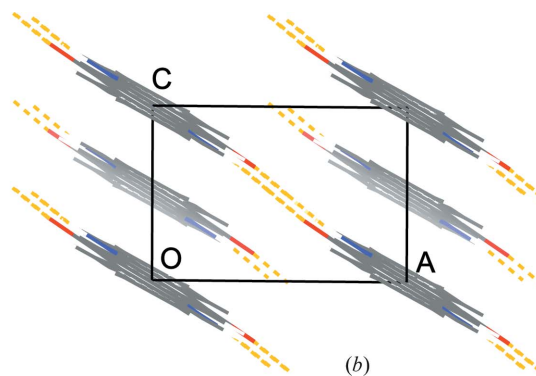
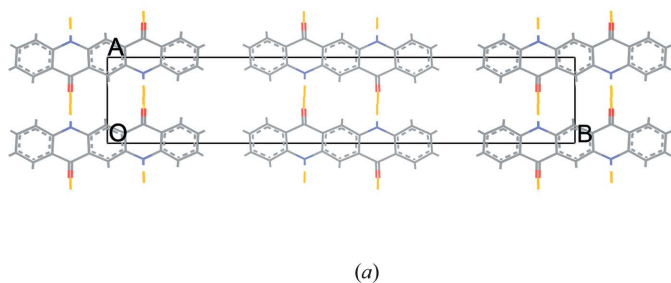
### 4.3. $\alpha$ -Quinacridone

The structure of  $\alpha$ -QA is deposited in the CSD under the reference code QNACRD03. It has been derived from the  $\gamma$ -QA structure by systematic variation of atomic coordinates (considering chemical bonding constraints) in order to fit the experimental powder pattern of  $\alpha$ -QA (Lincke & Finzel, 1996). The only difference with the  $\gamma$  structure is the angle between the molecules in the criss-cross arrangement. Using the Dreiding force field, we found that this structure converts during minimization readily to the structure of the  $\gamma$  polymorph; this makes the QNACRD03 structure questionable.

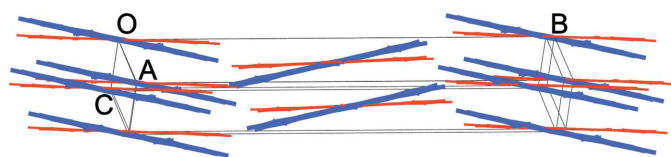
Several structures, with numbers 8–12 in Table 1, are predicted by the PP to have powder patterns similar to the experimental one (Fig. 11). Structures 8–11 are triclinic, space group  $P\bar{1}$ . Each quinacridone molecule shares hydrogen bonds

with two neighbours, forming ribbons similar to those in  $\beta$ -QA, along [100]. These are packed in such a manner that all molecules in the structure lie parallel to one another (Fig. 10). Structure 12 is monoclinic, space group  $P2_1$ , and it has a different packing motif. Crystallization of centrosymmetric molecules in a non-centrosymmetric space group is, however, very rare.

The quality of the experimental powder pattern was not high enough to obtain an acceptable fit of the patterns. Structures 10 and 11, as being closest to the experimental powder pattern, were used further for the Rietveld refinement. The refinement converged at  $R$  values of 19.6% and 21.4%, respectively, and produced the structures at substantially much higher energy as compared with the initial values (Fig. 2). Rietveld refinement of the structure 12 resulted in a

**Figure 8**

Two projections of the predicted crystal structure of  $\beta_3$ -QA: views along the short and long axes. Dashed yellow lines represent hydrogen bonds.

**Figure 9**

Structure of  $\beta_3$ -QA minimized in the force field (red) and after the Rietveld refinement (blue).

relatively low  $R$  value of 14.3%. Visual inspection of the resulting XRPD pattern showed, however, that the structure 12 fitted the experimental pattern badly, mainly due to the mismatch of the peaks in the area  $25\text{--}30^\circ$ . The low  $R$  value is misleading in this case.

Structure 10, showing the best Rietveld fit among all five structures for the  $\alpha$  polymorph, can be regarded as the closest to the experimental structure. It is debatable if such a high  $R$  value is acceptable to confirm the similarity of the predicted structure and the experimental one. A higher quality powder pattern, at least, is necessary to arrive at a better fit.

What are the other structures in Table 1? Showing no similarity with the known experimental powder patterns, they have molecular packing and hydrogen-bond patterns that are similar to the polymorphs discussed above. Structure 3 has a criss-cross molecular motif, similar to that of  $\gamma$ -QA, but its powder pattern is very different from the experimental one (Fig. 4). Structures 6 and 7, as  $\beta_1$ -QA, consist of hydrogen-bonded ribbons running in two directions. Structure 15

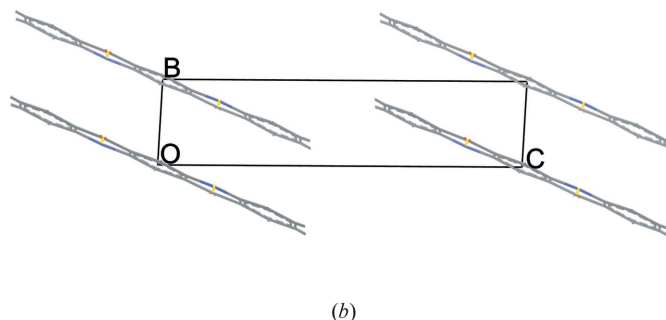
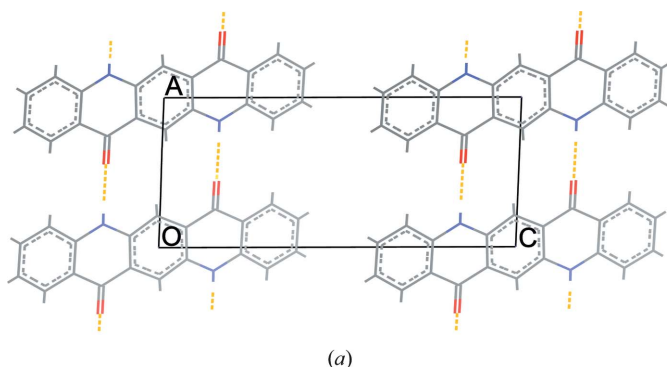
contains squeezed layers of molecular ribbons which resemble the packing of the  $\beta_2$  structure after the Rietveld refinement.

#### 4.4. Quality of the force field

An important question is how certain one can be of the results of the polymorph prediction approach outlined in this paper. The confidence in the results heavily depends on the quality of the force field and the atomic charges used.

The Dreiding force field (Mayo *et al.*, 1990), a generic force field, can be applied to a wide range of heteroatomic organic molecules with reasonable accuracy. It shows the best results when used with the charges derived from high-level quantum mechanics calculations (ESPD charges). It models hydrogen bonds in crystal structures reasonably well. In certain cases, for example hydrogen bonds in acids, limitations have been reported (Payne *et al.*, 1998). The force-field description of the structures in the present case appears to be quite adequate, since all three polymorphs were found within  $3\text{ kcal mol}^{-1}$ . Moreover,  $\gamma$ -QA, usually mentioned in the literature as a stable polymorph at room temperature, is found to have the lowest lattice energy.

If calculated lattice energies are close to the sublimation enthalpies, this can serve as another validation of the force field used. Lattice energy for the structures listed in Table 1 is  $50\text{--}53\text{ kcal mol}^{-1}$ . The sublimation enthalpy of quinacridone, as for many other pigments, is hard to measure due to the difficulties in precise measurements at high sublimation

**Figure 10**

Two projections of the predicted crystal structure of  $\alpha$ -QA. Dashed yellow lines represent hydrogen bonds.

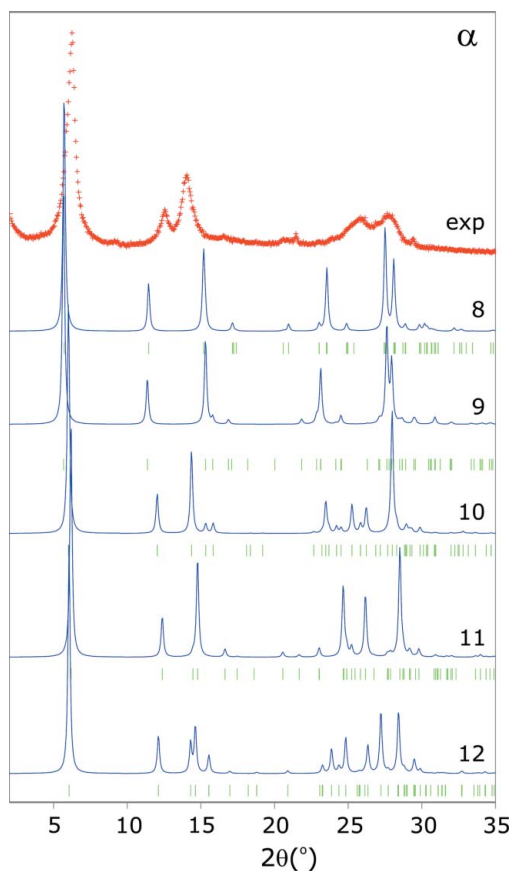


**Figure 11**  
Powder patterns of structures 8, 9, 10, 11 and 12 of Table 1 compared with the experimental powder pattern of  $\alpha$ -QA.

temperature. Therefore, no experimental data were found in the literature.

A number of promising developments have been reported in the area of force-field development, such as a better description of the electrostatics by means of a multipole expansion (van Eijck *et al.*, 2001), using a large number of charged cells to describe the charge density (Gavezzotti, 2002, 2003), or developing a tailor-made potential for the compound under investigation from quantum chemical calculations (Day & Price, 2003).

#### 4.5. X-ray powder data quality and limitations

As current progress in CSP showed, the problem in predicting is not the generation of all the possible structures (for that, present algorithms are good enough), but rather the ranking and choosing the right structures from the list. In the case of pure *ab initio* prediction, the first structure in the ranking is not always the experimentally stable polymorph. Here we combine *ab initio* CSP with experimental XRPD patterns to increase the chance of arriving at the right structure. Comparing powder patterns of predicted structures and experimental patterns usually shows large deviations. The differences arise from the limited prediction power of the force field and from the bad quality of the experimental diffraction pattern. An absolute match of the powder patterns

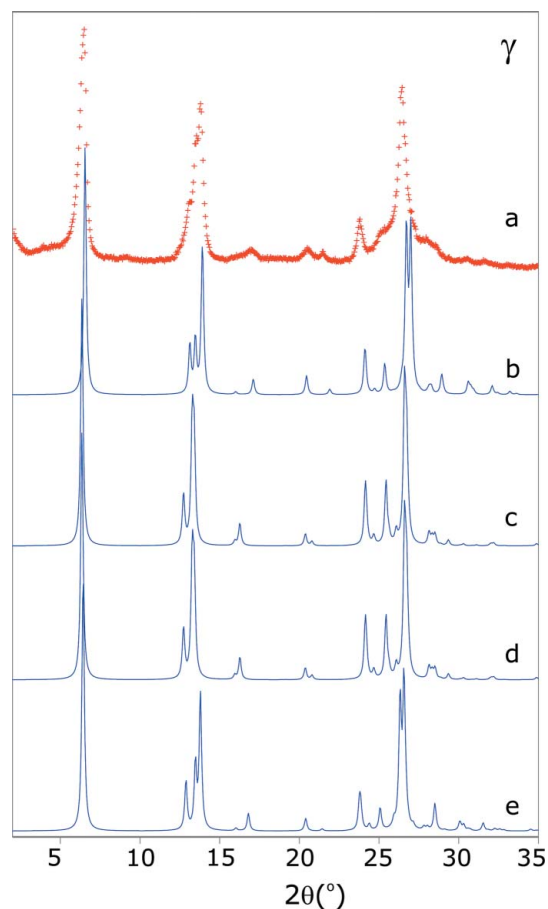


**Figure 12**  
Comparison of powder patterns of  $\gamma$ -QA: (a) experimental powder pattern, (b) calculated from experimental structure QNACRD04, (c) calculated from QNACRD04 after minimization in the force field, (d) calculated from structure 2, (e) calculated from structure 2 after Rietveld refinement (peak profiles not fitted for clarity).

in such cases is mostly regarded as a pure coincidence and is rather rare. Thus, the effectiveness of powder pattern comparison, in order to choose the right structures from the list of predicted ones, varies from case to case.

To get an impression of the deviation from the experimental pattern, it is interesting to compare powder patterns for  $\gamma$ -QA. Fig. 12 shows the experimental powder pattern together with four calculated ones, namely calculated from the CSD structure QNACRD04 before and after energy minimization in the force field, the powder pattern of structure 2 in the list of predicted structures (minimized), and that of structure 2 after Rietveld refinement against the experimental data. In this figure it is remarkable that the patterns (c) and (d) are identical. This means that the structure predicted by the PP is the same as the experimental structure minimized using the same force field and, therefore, it is probable that these two structures are also identical.

Fig. 12 also demonstrates how the effect of the force field leading to the difference between patterns (b) and (c) is eliminated by Rietveld refinement. Three peaks at 12–15° are overlapping in the experimental pattern (a) and distinct in the one calculated from the CSD structure (b). Due to the inac-

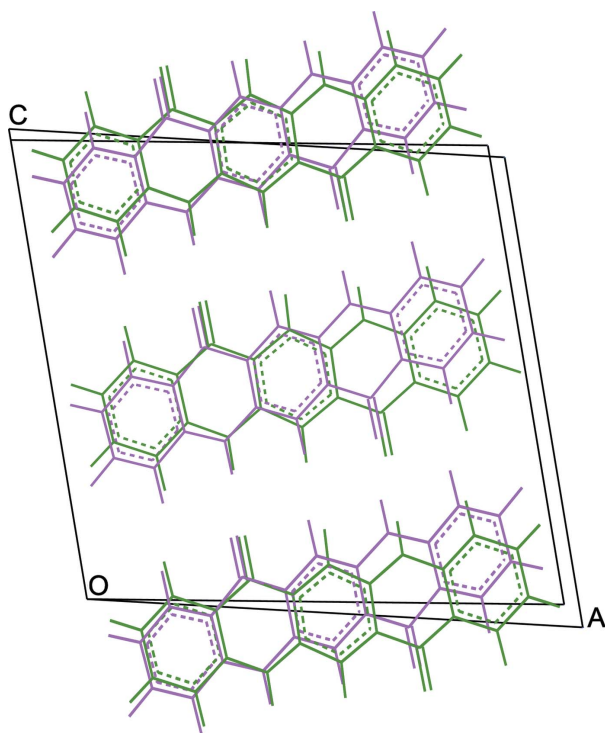


**Figure 13**  
Projection of the  $\gamma$ -QA structure QNACRD04 before (magenta) and after (green) energy minimization.

curacy of the force field, minimization of the energy results in changes in the structure (Fig. 13) and the three peaks merge into two in pattern (c). The predicted structure (d) also has two peaks in this area. After the Rietveld refinement three peaks are resolved again in the pattern (e). These five structures are assumed to be the same, but their powder patterns differ to a certain extent. This difference should be kept in mind when comparing other predicted structures with the experimental powder patterns.

Rietveld refinement is often used to complete the prediction procedure and to refine the trial structures against powder data. Full Rietveld refinement is, however, only worthwhile if the experimental data are of excellent quality (e.g. collected using synchrotron radiation) and the input structure is close enough to the experimental one. In the case of small particle size or poor crystallinity, like for many pigments, the low quality of the powder diffraction patterns cannot be improved by using more powerful X-ray sources. Moreover, Rietveld refinement is not efficient if the candidate crystal structure is not close enough to the experimental one and too few peaks in the simulated and experimental powder patterns exactly match (which happens very often).

An example of the intrinsic ambiguity of powder data can be found in the structure of  $\alpha$ -QA that was deposited in the CSD under the reference code QNACRD03 (Lincke & Finzel, 1996). This structure has a molecular packing very close to the criss-cross arrangement of molecules in  $\gamma$ -QA (and far from  $\alpha$ -QA, as predicted by us); only the angle between the molecules is different. However, this criss-cross  $\alpha$ -QA structure produces a powder pattern very close to the experimental pattern of  $\alpha$ -

QA, which leads to confusion. The reason to have more confidence in our variant of  $\alpha$ -QA is that it represents a real local minimum in a reliable force field.

In this case and in general, experimental X-ray powder diffraction patterns are not always unique ‘fingerprints’ of the crystal structures. Similarity of powder patterns of different polymorphs is not uncommon [for example, two polymorphs of terephthalic acid (Bailey & Brown, 1967; Brown, 1984)]. Thus, the methods that use the powder patterns or other types of experimental information solely to distinguish the polymorphs contain by default some degree of uncertainty. For more accuracy, a combination of different physico-chemical characterization methods should be applied.

#### 4.6. Stability order

Another indication of the quality of the present prediction is the stability order of the polymorphs. According to the calculated lattice energy of the structures, the order of descending stability for the predicted polymorphs is  $\gamma$ - $\beta$ - $\alpha$  or  $\gamma$ - $\alpha$ - $\beta$  (Table 1), depending on which structure to accept for  $\beta$ -QA. As was mentioned before, experimental data about the stability of these polymorphs are not available.  $\gamma$ -QA is often mentioned in the literature as the most stable form and  $\alpha$ -QA as the least stable form (Jaffe, 2001) ( $\alpha$ -QA is therefore not commercially important).

Moreover, during our crystal growth experiments by sublimation (Panina *et al.*, 2007), we observed that  $\beta$ -QA sublimed faster and at a lower temperature than  $\gamma$ -QA. This leads us to the conclusion that, at least at the temperature of sublimation (673 K), the  $\beta$  polymorph is less stable than the  $\gamma$  polymorph. Possibly,  $\beta$ -QA is less stable than  $\gamma$ -QA for the whole range of temperatures (monotropically related polymorphs), since no polymorphic transition could be observed till 773 K (Jones *et al.*, 1975). Assuming such a monotropic relation, our experimental data confirm the predicted stability order for  $\beta$ - and  $\gamma$ -QA.

The stable  $\gamma$  polymorph was ranked highest in the prediction. Experimentally observed metastable polymorphs, in general, are not necessarily next in this ranking, even in the case of perfect prediction results, as kinetics determine the circumstances under which they are formed and kinetics are not part of the prediction method.

## 5. Conclusions

The structures of three polymorphs of quinacridone were predicted using *Polymorph Predictor* in combination with XRPD patterns of limited quality. The known  $\gamma$  structure was predicted correctly as first in the ranking. Three different structures were proposed for the unknown  $\beta$ -QA that closely match the experimental powder pattern. For  $\alpha$ -QA, a better XRPD pattern is needed to obtain a reliable structure prediction.

The present work demonstrates a method to obtain crystal structures using *Polymorph Predictor* in combination with experimental XRPD patterns. *Ab initio* prediction (without

any help of additional information, like XRPD) is still not very reliable, even for simple molecules, mainly due to the limited quality of the force field. The use of X-ray powder data helps to improve the reliability of the prediction. Rietveld refinement can be used to improve the result. The effectiveness of the latter step is limited by the flexibility of the molecule and/or the quality of the XRPD pattern.

In the present prediction method, the XRPD pattern need not be indexable. We expect this method to be useful in the case of rigid organic molecules, if a corresponding non-indexable powder pattern of reasonable quality is available. Pigments are a good example of the application of this method, since pigment molecules are often rigid and XRPD patterns of pigments are usually difficult to index because of the peak broadening as a result of small crystal sizes.

*Note added in proof.* While the paper was in press, another paper on the single-crystal X-ray structure determination of  $\beta$ -quinacridone was published (Nishimura *et al.*, 2006). The structure reported in this paper fits very nicely our  $\beta_1$ -structure, which is the highest in ranking for the predicted  $\beta$ -structures.

This work is supported by the Institute for the Promotion of Innovation by Science and Technology in Flanders (IWT).

## References

- Accelrys (2002). *Cerius<sup>2</sup>*, version 4.71, *User Guide*. Accelrys Inc., San Diego, USA.
- Bailey, M. & Brown, C. J. (1967). *Acta Cryst.* **22**, 387–391.
- Baur, W. H. & Kassner, D. (1992). *Acta Cryst.* **B48**, 356–369.
- Brown, C. J. (1984). *Acta Cryst.* **C40**, 1762.
- Day, G. M. *et al.* (2005). *Acta Cryst.* **B61**, 511–527.
- Day, G. M. & Price, S. L. (2003). *J. Am. Chem. Soc.* **125**, 16434–16443.
- Deuschel, W., Gundel, F., Wuest, H. & Daubach, E. (1963). US Patent 3074950.
- Eijck, B. P. van, Mooij, W. T. M. & Kroon, J. (2001). *J. Comput. Chem.* **22**, 805–815.
- Erk, P. (2001). *High Performance Pigments*, edited by H. M. Smith, ch. 8, pp. 103–123. Weinheim: Wiley-VCH.
- Filho, D. S. & Oliveira, C. M. F. (1992). *J. Mater. Sci.* **27**, 5101–5107.
- Frisch, M. J. *et al.* (1998). *GAUSSIAN94* (Revision D.4), Gaussian Inc., Pittsburgh, USA.
- Gavezzotti, A. (2002). *J. Phys. Chem. B*, **106**, 4145–4154.
- Gavezzotti, A. (2003). *J. Phys. Chem. B*, **107**, 2344–2353.
- Gdanitz, R. J., Karfunkel, H. R. & Leusen, F. J. J. (1993). *J. Mol. Graph.* **11**, 275–276.
- Jaffe, E. E. (2001). *High Performance Pigments*, edited by H. M. Smith, ch. 18, pp. 279–306. Weinheim: Wiley-VCH.
- Jones, F., Okui, N. & Patterson, D. (1975). *J. Soc. Dyers Col.* **91**, 361–365.
- Karfunkel, H. R., Leusen, F. J. J. & Gdanitz, R. J. (1994). *J. Comput. Aided Mater. Des.* **1**, 177–185.
- Karfunkel, H. R., Rohde, B., Leusen, F. J. J., Gdanitz, R. J. & Rihs, G. (1993). *J. Comput. Chem.* **14**, 1125–1135.
- Leusen, F. J. J. (1996). *J. Cryst. Growth*, **166**, 900–903.
- Lincke, G. (2000). *Dyes Pigments*, **44**, 101–122.
- Lincke, G. & Finzel, H. U. (1996). *Cryst. Res. Technol.* **31**, 441–452.
- Manger, C. W. & Struve, W. S. (1957). US Patent 2844581.
- Mayo, S. L., Olafson, B. D. & Goddard, W. A. III (1990). *J. Phys. Chem.* **94**, 8897–8909.
- Mizuguchi, J., Sasaki, T. & Tojo, K. (2002). *Z. Kristallogr.* **217**, 249–250.
- Nishimura, N., Senju, T. & Mizuguchi, J. (2006). *Acta Cryst.* **E62**, o4683–o4685.
- Panina, N., Janssen, F. F. B. J., Deroover, G., Meekes, H. & Vlieg, E. (2007). In preparation.
- Paulus, E. F., Dietz, E., Kroh, F., Prokschy, F. & Lincke, G. (1989). *12th European Crystallographic Meeting*, published in *Z. Kristallogr.* (1990, Suppl. 2), pp. 23–24.
- Payne, R. S., Roberts, R. J., Rowe, R. C. & Docherty, R. (1998). *J. Comput. Chem.* **19**, 1–20.
- Potts, G. D., Jones, W., Bullock, J. F., Andrews, S. J. & Maginn, S. J. (1994). **22**, 2565–2566.
- Reidinger, A. D. & Struve, W. S. (1955). US Patent 2844484.
- Schmidt, M. U., Ermrich, M. & Dinnebie, R. E. (2005). *Acta Cryst.* **B61**, 37–45.
- Struve, W. S. (1955). US Patent 2844485.
- Wiles, D. B. & Young, R. A. (1981). *J. Appl. Cryst.* **14**, 149–151.